ISSN 1061-933X, Colloid Journal, 2014, Vol. 76, No. 5, pp. 564–575. © Pleiades Publishing, Ltd., 2014.

Aggregates of Poly-Functional Amphiphilic Molecules in Water and Oil Phases[1]

K. Kovalchuk[a], E. Riccardi[b,] *, A. Mehandzhiyski[a], and B. A. Grimes[a]

[a] *Ugelstad Laboratory, Department of Chemical Engineering, Norwegian University of Science and Technology Sem Sælands vei 4, NO-7491 Trondheim, Norway*

[b] *Current address: Department of Chemistry, Norwegian University of Science and Technology, Högskoleringen 5, 7491 Trondheim, Norway*

**e-mail: e.riccardi82@gmail.com*

Received January 30, 2014

Abstract—The solvation and aggregate formation of complex amphiphilic molecules such as tetra-acids in polar and nonpolar phases are studied via Molecular Dynamics simulations. The nonpolar core of tetra-acid molecules is found to be effectively impermeable for water molecules resulting in a low solubility in the polar solvent, while nonpolar solvent molecules sufficiently solvate the amphiphilic molecules considered, enabling an open conformation of their molecular structure. The rigidity of the core region of the tetra-acid molecules has been found to play a crucial role in their behavior in both polar and nonpolar phases. In the polar phase, simulations have shown that tetra-acids form micelle-like structures with a small aggregation number, confirming previous experimental work. The identification of a case of study in which micelle-like structures can form only with a small aggregation number enables the study via Molecular Dynamics of micelle–micelle interactions. Micelle stability and dispersion in the polar phase under different conditions can be therefore investigated. In the nonpolar phase, the preferential interactions between carboxyl groups, the affinity of the tetra-acids with the solvent molecules, and the structural characteristics of the central core moiety of the tetra-acids have been found to possibly induce a web like array, or network.

DOI: 10.1134/S1061933X1405010X

INTRODUCTION

Micelles can be found in a large variety of systems due to the abundance of natural and synthetic amphiphilic molecules and the understanding of micelle properties is essential in fields involving emulsions and liquid-liquid separations [1–4]. Micelle properties, such as shape, dimension, concentration, dispersion state, etc. depend on a large amount of variables like temperature, pressure, solvent type, pH, ionic strength, counter-ion type, and the chemical and ternary structure of the constituent amphiphilic molecules [1–8]. Molecular Dynamics (MD) simulations and other computer experiments [3, 4] have been widely used to study the physicochemical and thermodynamic properties of amphiphilic molecules as well as their self-assembly. Simulations have described how different properties of the amphiphilic molecules and of the system, e.g. pH, ionic strength, can lead to different micelle shape, dimension, and growth rate [3–8]. MD simulations have also shown the influence of the counterions on micelles, reporting how different counterions can alter their growth process [4]. However, a drawback of using MD to study micelles is that the study of large aggregates can result in exceedingly demanding simulations due to the system dimensions. Furthermore, as a consequence of the polar nature of the system and the importance of the partial charges on the amphiphilic molecules and ions in the local environment, full atomistic MD simulations should be employed to provide crucial dynamic system details which cannot be included by coarse grain model simulations although the later would require shorter simulation times. While the properties of small aggregates of linear amphiphilic molecules have been widely investigated, few investigations of aggregates of multifunctional nonlinear amphiphilic molecules have been studied by MD simulation [9].

In crude oil, naphthenic acids are present at low concentration [2, 5, 10]. Their amphiphilic properties are known to cause significant environmental and economic problems in the crude oil processing chain. On the other hand, their complex structure and polyfunctional characteristics could be advantageously exploited in other applications/fields. In the present work, two tetra-acids (TAs) have been considered. The first is a C_{80}-tetrameric carboxylic acid molecule, which is a compound occasionally found indigenously in acidic oil reserves and is commonly referred to as ARN [5, 10, 11]. The second TA here considered is a model compound of ARN, named BP10, which has been synthesized by Nordgård and Sjöblom [12]. BP10 has a structure similar to ARN and is able to

[1] The article is published in the original.

mimic several of its interfacial and bulk properties [13]. Their difference is mainly in the chemical structure of the central cores, which could potentially generate different aggregate structures. Due to the complex structure of the constituents, such aggregates can differ significantly from aggregates formed by linear amphiphilic molecules in both polar and nonpolar phases. Recently, Ge et al. [14] have investigated self-association properties of fully ionized BP10 in aqueous solution using dynamic light scattering (DLS). Micelles have been detected with diameters in the range between 2 and 6 nm [14–16]. Complementary experiments using small-angle neutron scattering (SANS) were performed by Simon et al. [15] to compare the aggregation of fully ionized ARN and BP10 molecules. For BP10, micelles formed at low salt concentration with aggregation numbers in the range of 4–5; these results were in agreement with the DLS study. At low ionic strengths, ARN had been found to form bigger aggregates than BP10; the large size of these aggregates could not be determined due to the low resolution of the performed SANS measurement. In addition, a clear conclusion about the formation of ARN aggregates could not be formulated due to the excessive presence of impurities that interact with the TAs in the investigated sample altering their behavior [15].

MD simulations have been successfully employed to simulate ARN and BP10 at the interface between a polar and nonpolar solvent [6]. The results consistently showed that such TAs behave differently from common linear amphiphilic molecules at the interface between the solvents. This finding suggested the study of aggregates of these complex molecules in both the bulk polar and nonpolar phases. Therefore, in the present work, MD simulations have been performed to simulate and identify the aggregates that ARN and BP10 can form in polar and nonpolar bulk phases. The main difference between BP10 and ARN is the number of rotational degrees of freedom for the atoms in the central core moieties of the molecules. Specifically, bond rotations for the carbon atoms in the two unsaturated ring structures of the BP10 core are restricted, while all atoms in the ARN core structure have some rotational degrees of freedom. The different accessible conformational space of the core structures result into a different structural rigidity, which should be reasonably considered a determinant in the formation of aggregates. The common similarity of these amphiphilic molecules is their polar head groups located at the extremes of the molecule, and the non-polar or weakly polar section in their core. Such a description of the TA molecules is similar to the description of a micelle given above. In this perspective, the aggregation process of a few TA molecules could, in principle, resemble the micelle aggregation process. If that hypothesis is confirmed, a very small number of molecules would be necessary to form micelle-like structures and possibly aggregates of these structures. Consequently, TA molecules could provide a case of study for a micelle system with a small aggregation number that could be extremely useful for study by MD simulation. A relatively small number of amphiphilic molecules and solvent molecules would be required to be included in the simulation and less demanding simulations can enable the direct simulation and study of processes such as micelle growth, micelle stability, and micelle aggregation etc. as a function of various system variables of interest. The reduced size of the system would also allow one to maintain the required level of full atomistic resolution to properly consider the effect of partial charges, dipole and quadrupole moments present in the amphiphilic molecules as well as counterion and solvent molecules.

In the nonpolar phase, amphiphilic molecules are known to form, in suitable conditions, inverse micelles [1]. However, the dimension of the non-polar central core is expected to play a predominant role dictating the properties of these amphiphilic molecules in the bulk nonpolar phase. It appears unlikely to observe the formation of compact aggregates. On the other hand, due to the affinity of the polar sites of the amphiphilic groups, super molecular structures could be generated in the oil phase. Therefore, the TA behaviors, and their mutual interactions, have also been investigated in the present work, via MD, in a nonpolar solvent.

2. MODELS AND METHODS

Molecular Dynamics simulation in full atomistic resolution has been employed to simulate ARN and BP10 tetra-acids. The molecules have been simulated according to the OPLS-AA force field [17] in their protonated (uncharged) and deprotonated (charged) states. OPLS-AA has been developed by fitting the experimental properties of liquids, and it includes all the intra- and inter-molecular interaction potentials and parameters for the molecules here considered. In the charged state, electroneutrality has been guaranteed by four sodium counter-ions, Na^+, for each TA molecule to compensate the charges of the deprotonated carboxyl groups. The counter-ion has been modeled as a single charged particle according to the OPLS-AA force field with a +1 net charge located in the center of the bead. The TA molecules have been simulated in their uncharged state in a nonpolar solvent and in their charged state in a polar solvent. A mixture of *p*-xylene/$CHCl_3$ 9 : 1 vol/vol has been chosen as the nonpolar solvent based on the solubility of BP10 [12], while water is the polar solvent. The nonpolar phase has been selected for consistency with previous simulations [6] and experiments [14, 15]. It should be noted here that from this point forward, the nonpolar phase will be referred to as an "oil" phase for convenience although strictly speaking the nonpolar phase of *p*-xylene and chloroform is not an oil. Consistent with the TAs, *p*-xylene and $CHCl_3$ have been modeled in full atomistic details with the OPLS-AA force field [17] while water has been modeled with the

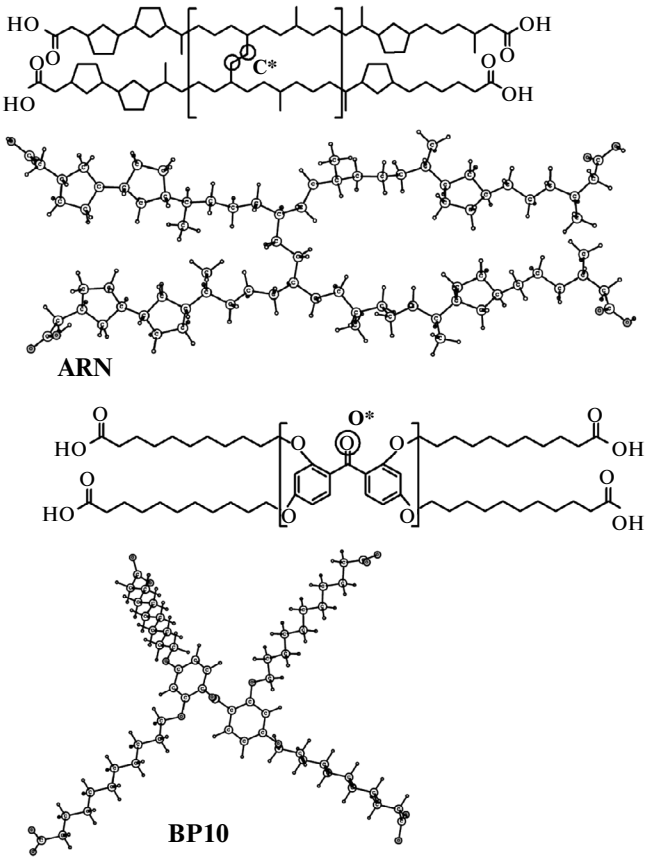

Fig. 1. Chemical structure diagrams and ball and stick models for ARN and BP10. On the chemical structure diagrams, the central atoms used in the RDF's are indicated with a circle and the central core groups are in brackets.

TIP4p/2005 force field [18]. All the simulations have been performed with the GROMACS 4.5 simulation package [19]. A temperature of 300 K and a pressure of 1 bar have been controlled in the *NPT* ensemble via a velocity rescaling method [20] and the Berendsen barostat, respectively. Particle-Mesh Ewald summation has been selected for the electrostatic interactions and a cut off distance of 1.2 nm has been chosen for the non-bonded interactions. Periodic boundary conditions have been applied along all three dimensions, and the Leapfrog algorithm has been selected to integrate Newton's equation of motion with a 1 fs time step interval.

The two bulk phases considered have been studied in two independent simulation sets. For the nonpolar (oil) solvent, 2256 and 315 *p*-xylene and $CHCl_3$ molecules have been employed and randomly positioned in a large simulation box, while 10000 water molecules have been employed for the polar solvent. The representative oil and water bulk phases have thereafter been equilibrated to ambient conditions. A TA molecule, previously equilibrated in vacuum, has been replicated into a 3D homogeneous distribution with a random orientation obtaining the desired molecule number for each case. Both ARN and BP10 are studied in each solvent at 4 different loads: 1—case (i), 2—case (ii), 4—case (iii) and 8 molecules—case (iv). The equilibrated bulk phases and the TA systems were then combined, superimposing the molecular positions. The overlapping solvent molecules have been thereafter relocated. This procedure generated a total of 16 systems, 8 for ARN and 8 for BP10. Considerations on the dependence of the results upon the selection of the initial conditions will be addressed in the Results and Discussion section.

Each system has been then independently equilibrated in a *NPT* ensemble. A temperature and pressure annealing procedure has been adopted. For 1 ns, the systems have been kept at 400 K and 100 bar and then progressively relaxed to ambient conditions with a transition time of 5 ns. Once ambient conditions have been reached, an additional 10 ns has been simulated before initiating the system sampling. The sampling has been performed for a period of 10 ns in 2.5 ps intervals. The resulting dimensions of the simulation boxes for the different systems are about $8 \times 8 \times 8$ nm^3—or the oil bulk, and about $7 \times 7 \times 7$ nm^3 – for the water bulk.

3. RESULTS AND DISCUSSION

A full atomistic molecular representation of the tetra-acids considered in the present work is reported in Fig. 1. The two TAs have a similar general structure where a core group is connected to four hydrocarbon chains (arm groups) that terminate with a carboxylic acid moiety. They differ mainly in the central core which is composed of a benzophenone group for BP10 and by saturated hydrocarbons for ARN. It is important to stress here that the ARN molecule has two distinct arm groups that contain saturated cyclical rings while BP10 has four identical linear arm groups. The carboxyl acid groups have been considered fully protonated in the oil phase and fully deprotonated in the water phase.

3.1. Solvation

Figure 2 provides insight into the conformation of the TAs in the different solvents. The radial distribution function (RDF) around the carbon atom of the carboxyl groups, $g^{COO^-–COO^-}(r)$, for one molecule of either TA—case (i) and the RDF of the carbon atoms of the carboxyl groups around the TA central atoms, $g^{Center–COOH}(r)$ in water has been reported in Figs. 2a and 2b, respectively (the "center" atoms are defined by the circled atoms, C* and O*, for ARN and BP10, respectively, indicated in Fig. 1). Analogous distributions have been also been reported for the nonpolar solvent, Figs. 2c and 2d. The vertical lines in Figs. 2b and 2d represent the mean values of the RDF's between the center atoms and the carboxylate groups. In Fig. 2a, it can be noted that in water the carboxyl

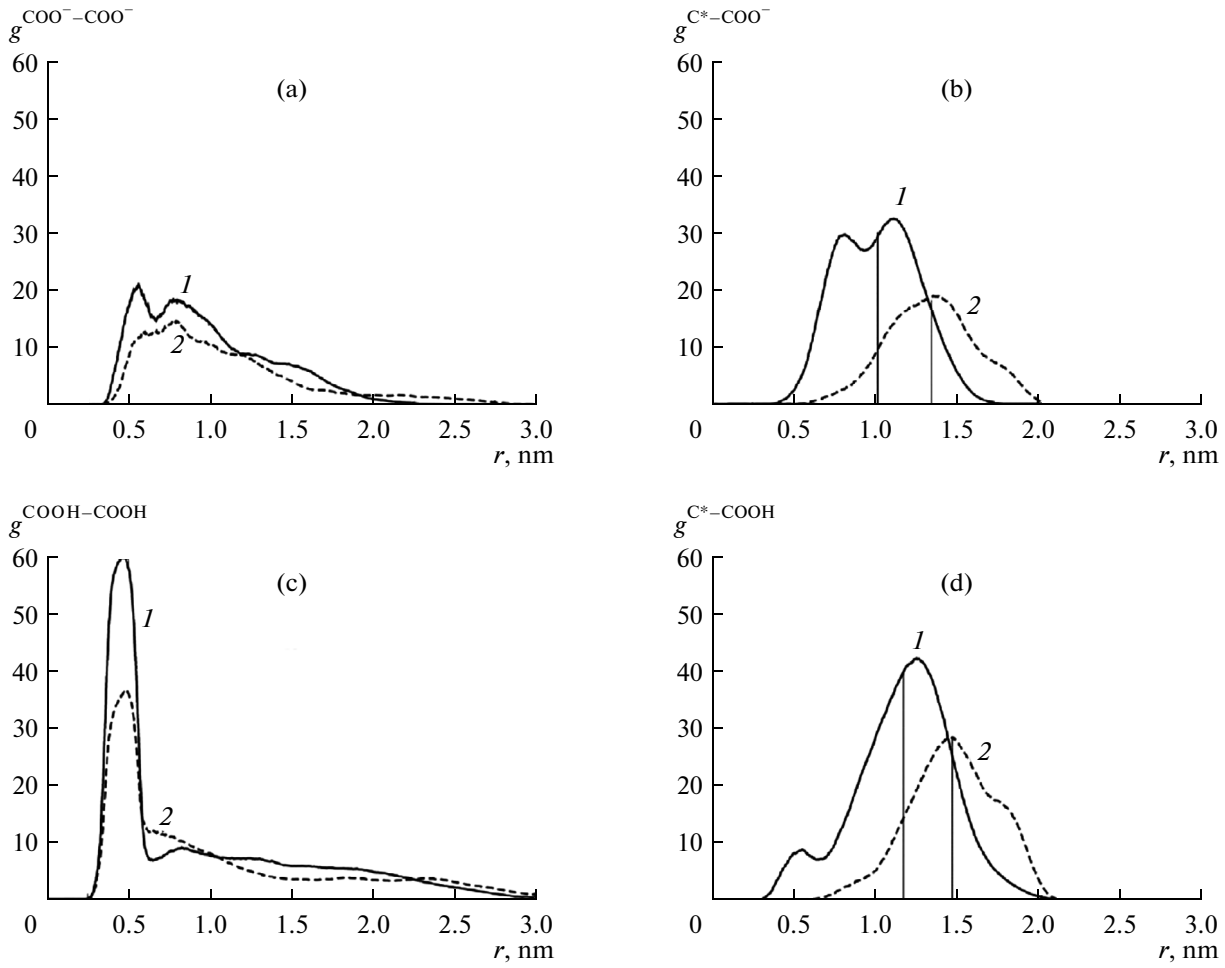

Fig. 2. RDFs for case (i). (a)—$g^{COO^-–COO^-}(r)$, for ARN (*1*) and for BP10 (*2*), (b)—$g^{C^*–COO^-}(r)$ for ARN (*1*) and for BP10 (*2*) in water phase; (c)—$g^{COOH–COOH}(r)$ for ARN (*1*) and BP(*2*), (d)—$g^{C^*–COOH}(r)$ for ARN (*1*) and $g^{O^*–COOH}(r)$ for BP10 (*2*) in the bulk oil phase. The vertical lines in (b) and (d) mark the location of the mean value of the distributions.

groups of the two TAs assume a relatively similar distribution. The main difference between ARN and BP10 in the water solvent can be observed in Fig. 2b. ARN presents a double maximum, symptomatic of the different length of its arms, while BP10 tends to uniformly position its carboxyl groups at higher distances with respect to the center of the molecule. In the oil solvent, it can be observed from Fig. 2c that ARN and BP10 tend to position their carboxylic acid groups in a prevailingly coupled state, as shown by the maximum present at 0.5 nm. In the radial distribution profile for ARN, a local minimum is present at 0.65 nm while an almost linear decay is shown by the BP10 radial distribution profile. This can be interpreted as a higher stability of the ARN carboxyl group pairs while BP10 seems to form and break the carboxyl pairs with a higher probability. Generally, it can be stated that BP10 tends to assume generally a more open configuration with respect to ARN in both water and oil bulk. Both ARN and BP10 tend to form a more compact structure in the water phase (bad solvent) relative to the oil phase (good solvent), confirmed with a difference of about 10% in the mean value of the respective RDFs in the different solvents. It should be noted that the magnitude of the maxima of RDF plots is consequence of the normalization factor of RDF—bulk density—that is computed by the spherical integral of the RDF. In the cases where there is a relative modest presence of particles at long distances (here excluding periodic images), a rather large maxima shall be expected.

Changing perspective, the effects of the solvent can be investigated by studying the RDF's of the TAs with the water and oil molecules, which is described in Fig. 3 for both TAs. Figures 3a and 3b present the RDF's of atoms of water around the charged carboxylic acid groups (COO^-), and the central core structures (as indicated by the bracketed moieties in Fig. 1) for both ARN and BP10 in the bulk water phase. Figures 3a and 3b additionally present the RDF's between sodium ions and the charged carboxylic acid groups. It is

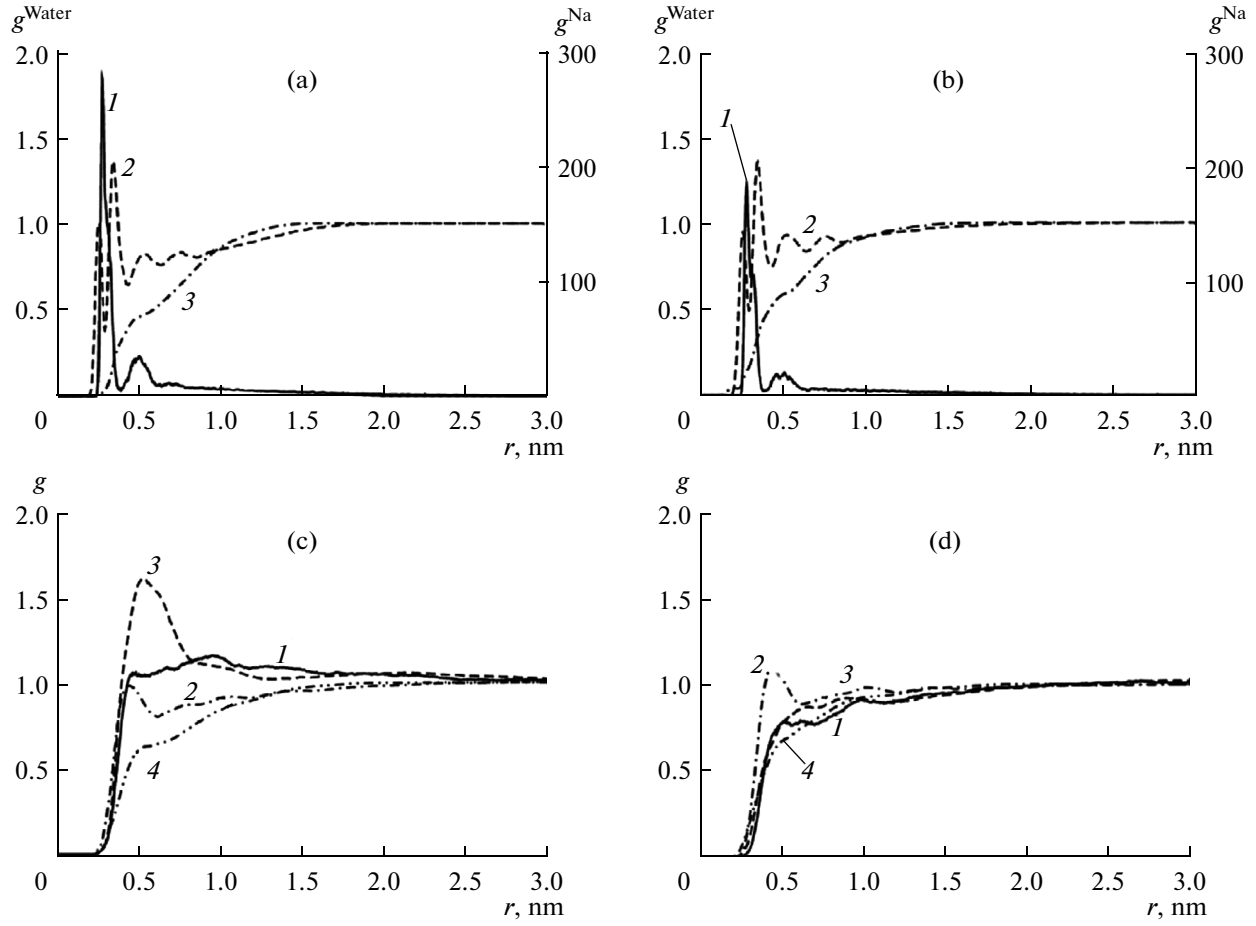

Fig. 3. RDFs for case (i) in the bulk water (a, b): *1*—$g^{COO^-–Na^+}(r)$, *2*—$g^{COO^-–Water}(r)$, *3*—$g^{Core–Water}(r)$: in the oil phase (c, d): *1*—$g^{COOH–CHCl_3}(r)$, *2*—$g^{COOH–Xylene}(r)$, *3*—$g^{Core–CHCl_3}(r)$, *4*—$g^{Core–Xylene}(r)$.

clear from Figs. 3a and 3b that water can reach the proximity of the carbon in the carboxyl group and, thereafter, form well defined solvation shells at about 0.35, 0.5 and 0.8 nm. However, there are no observable structures of water around the central core moieties. A few water molecules can be found in proximity of the BP10 core and, generally, it appears that the BP10 core is slightly more permeable to water than the ARN core. The progressive increase of the water concentration with increasing distance from the TA core is consistent with a compact molecular conformation. The RDF's in Figs. 3a and 3b indicate that there are well-structured sodium ion concentration shells around the COO^- groups for both TA molecules in the bulk water phase. A strong peak occurs at about 0.3 nm along with a second well defined peak at about 0.5 nm. The RDF, $g^{COO^-–Na^+}(r)$, shows alternating regions of higher Na^+ and water concentration. There is, therefore, a concurrence and an excluding volume effect between the solvent molecules and the counter ions. This suggests that for different counter ions, the solvation and, therefore, the induced TA structures could be modified by different counter ions characteristics. The net local minimum between the two peaks indicates that the carboxyl/sodium pair, once formed, has a low probability to be split. By comparing Figs. 3a and 3b, it is possible to conclude that this behavior is almost identical for ARN and BP10. It can be noted from Figs. 2a, 2b and 3a, 3b that the two different amphiphilic molecules tend to behave like a micelle of very small dimension (sub-micellar aggregate). A clear separation between water molecules and the hydrophobic core structures can be observed when the polar groups are positioned in the outer part of the monomolecular structure while strong interactions with local counterions occur.

In Figs. 3c and 3d, the RDFs of the atoms of the oil solvent molecules (xylene and $CHCl_3$) around the carbon atom of the carboxylic acid groups, and around the atoms of the central core structure of ARN and BP10 are presented, respectively. The results reported in Fig. 3c suggest that $CHCl_3$ interacts directly with the central core group of the ARN molecule as indi-

cated by the local maximum of $g^{\text{Core–CHCl}_3}(r)$ at 0.5 nm and by the following local concentration decay up to a distance of 1.25 nm. The near linear decay could be a consequence of a preferential interaction between the ARN cores with $CHCl_3$ molecules even at long range. The $g^{\text{Core–Xylene}}(r)$ spatial profile indicates that there is an unfavorable interaction between xylene and the ARN core. On the other hand, Fig. 3d indicates that there is only a modest preferential interaction between the BP10 core and $CHCl_3$ with respect to xylene. Both TA central cores do not allow xylene to find a coordination state in the bulk oil phase, causing a lower xylene local density up to a distance of 1.5 nm. It can be inferred that this effect could be caused by the steric and structural rigidity of the TA central core and xylene. In Figs. 3c and 3d, a higher concentration of $CHCl_3$ around the protonated carboxylic acid groups (COOH) in ARN relative to BP10 is reported. This could reasonably be due to the higher local concentration of chloroform induced by the ARN core. For both ARN and BP10, a local minimum in the $g^{\text{COOH–Xylene}}(r)$ occurs around 0.5 nm, which indicates a preferential interaction between protonated carboxyl groups and xylene. These weak solvent coordination structures are consistent with the extremely poor solubility of BP10 in many solvents [17].

3.2. ARN and BP10 Aggregates in Water

The aggregation process can be studied by successive simulations with an increasing number of amphiphilic molecules (tetra-acid molecules). To facilitate the discussion and description of the results for water and oil solvents, cases (i–iv) will be used to indicate the different systems where different amounts of either ARN or BP10, have been considered. As mentioned above in section 2, case (i) refers to one amphiphilic molecule in the system, case (ii) corresponds to 2 molecules, case (iii) represents 4 molecules and case (iv) refers to the 8 molecule system.

In Figs. 4a and 4b, the aggregates have been described by a set of radial distribution functions of the various system components with respect to the aggregate center of mass (ACOM). Such RDF's with respect to the individual TA molecules and water molecules are presented, while in Figs. 4c and 4d the RDF's with respect to Na^+ and the carbon atom of the COO^- are reported for ARN and BP10, respectively. From the RDF's, it can be inferred that ARN generates a net phase separation between its hydrocarbon region and the water phase for all the cases considered (ii–iv). Between the two phases, an over-concentration of COO^- and Na^+ ions is present forming an interphase region which is locally non electroneutral. Upon increasing the number of amphiphilic molecules within the range considered, the non-polar phase grows in dimension. The interface recedes from the center of the aggregate along with most of the COO^- and Na^+ groups. No water molecules can be found close to the center of the aggregate cores, with the exception for case (iv) for BP10. BP10 shows a similar behavior for aggregates composed of 2 and 4 molecules as shown by Figs. 4b and 4d, however, when 8 molecules – case (iv) – have been considered, the radial distribution functions $g^{\text{ACOM–Na}^+}(r)$ and $g^{\text{ACOM–COO}^-}(r)$ show a relatively low concentration of TAs in the center of the generated aggregate. BP10 tends to accumulate around 0.5 nm from the center of mass of the aggregate. Ionic groups, instead, can be found in high concentration close to the ACOM. This description suggests that the latter BP10 aggregate is not homogenous and for a full description of its properties additional descriptions will be provided in the forthcoming paragraphs. The internal aggregate conformation of ARN and BP10 is elucidated by Fig. 5, where the mutual distribution of the TAs is described through the RDF's, $g^{\text{C*–C*}}(r)$ and $g^{\text{O*–O*}}(r)$, and $g^{\text{COO}^-\text{–COO}^-}(r)$. For ARN, as shown by the maxima of $g^{\text{C*–C*}}(r)$ around 0.5 nm reported in Figs. 5a–5c, the tendency to generate a compact structure is noticeable. The RDF's also show that the dimension of the aggregate progressively and uniformly increases with the number of the molecules present in the system, and is consistent with the observations previously described in Figs. 4a and 4c. In particular, Fig. 4c shows how the electric double layer is progressively moving for higher aggregation numbers from the center of the aggregate. Such growth processes are also illustrated by Fig. 6, where a snapshot is reported for different aggregate dimensions. Comparing the magnitude of the peaks in $g^{\text{C*–C*}}(r)$ and $g^{\text{COO}^-\text{–COO}^-}(r)$ reported in Figs. 5a–5c, it appears that the carboxyl groups have a relatively smaller contribution to the formation of the aggregate, while the greatest contribution is provided by the core moiety of the TA. As demonstrated by $g^{\text{O*–O*}}(r)$ and $g^{\text{COO}^-\text{–COO}^-}(r)$, BP10 has a similar behavior for low aggregation numbers. However, in the aggregate formed by 8 BP10 molecules, instead, the rigid structure of the TA cores does not allow the formation of a uniform compact aggregate. The presence of water molecules in the central core, as previously discussed and shown by Fig. 4b, and the presence of two peaks in $g^{\text{O*–O*}}(r)$—Fig. 5c—clearly confirms the presence of two different aggregates of BP10 molecules in case (iv). The magnitude of the peaks in the $g^{\text{COO}^-\text{–COO}^-}(r)$ indicates that the two sub-aggregates interact mainly via the carboxyl groups. The resulting structure can also be visualized from the snapshot reported in Fig. 6. Concluding, it appears that both ARN and BP10 can form small micelle-like structures. In the aggregation number range studied, ARN forms roughly spherical aggregate structures which appear to be able to further

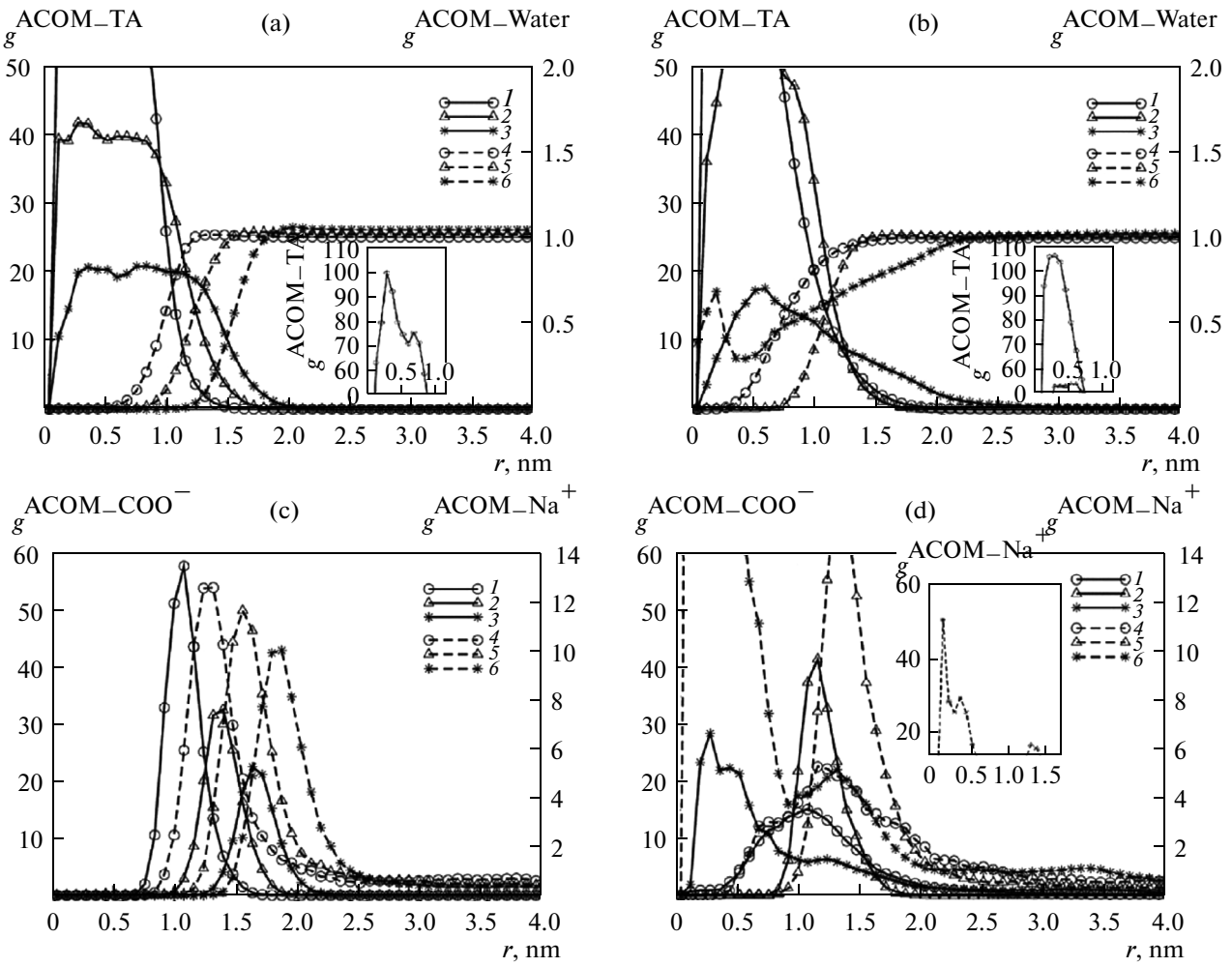

Fig. 4. RDFs for the center of mass of ARN (a) or BP10 (b) aggregates with individual ARN/BP10 molecules or water molecules in the bulk water phase: *1*—$g^{\text{ACOM–TA}}(r)$ for 2 TA molecules, *2*—$g^{\text{ACOM–TA}}(r)$ for 4 TA molecules, *3*—$g^{\text{ACOM–TA}}(r)$ for 8 TA molecules, *4*—$g^{\text{ACOM–Water}}(r)$ for 2 TA molecules, *5*—$g^{\text{ACOM–Water}}(r)$ for 4 TA molecules, *6*—$g^{\text{ACOM–Water}}(r)$ for 8 TA molecules. RDFs for the center of mass of ARN (c) or BP10 (d) aggregates with the carboxyl groups of the individual TA molecules or sodium ions in the bulk water phase: *1*—$g^{\text{ACOM–COO}^-}(r)$ for 2 TA molecules, *2*—$g^{\text{ACOM–COO}^-}(r)$ for 4 TA molecules, *3*—$g^{\text{ACOM–COO}^-}(r)$ for 8 TA molecules, *4*—$g^{\text{ACOM–Na}^+}(r)$ for 2 TA molecules, *5*—$g^{\text{ACOM–Na}^+}(r)$ for 4 TA molecules, *6*—$g^{\text{ACOM–Na}^+}(r)$ for 8 TA molecules.

increase their dimensions. BP10, instead, seems to form aggregate structures only with a very low aggregation number. This result supports the experimentally measured aggregation number [15]. BP10 micelles, for the selected case of study, appear to cohere to each other, resulting in an aggregate of aggregates. It should be noted that the focus of the present work is the study of the formation of micelles and the definition of an advantageous template to which further investigations can be referred. Micelle formation and growth, especially at such low aggregation number, is dependent on the path on which micelles enter into contact with other constituent molecules. The dependence of micelle formation on the initial conditions of the simulation would therefore result in a probability distribution for the aggregation number of the micelle. Such an aggregation number distribution would enhance the resolution of the present study, but is beyond the scope of the present work. Here a deeper insight into the TA micelle formation mechanism has been provided and a representative case of study that can enable further investigations on micelle–micelle interaction established. The definition of a case of study where micelles of very small dimension can be found it is an advantageous reference and starting point for MD simulations and statistical mechanics models. It should also be noted that the rate of growth of the aggregates, which is of interest, is dependent on the initial concentration

of TA molecules and on the magnitude of its self-diffusion in the different solvents. While such a perspective is of interest, it shall be addressed in forthcoming investigations where essential factors such as salt concentration, counterion type, pH, temperature, pressure etc. shall be included.

3.3. ARN and BP10 Aggregates in Oil

In oil phase, BP10 has been found to show a tendency to locally overconcentrate forming an aggregate structure which apparently differs from the ones identified in the water phase. Figure 7 reports the radial distribution function, centered on the ACOM with respect to the TA atoms and oil molecules. In Fig. 7, it can be noted that the concentration of the solvent is very little affected by the presence of the aggregate. BP10, for cases (iii) and (iv), shows a semi-constant concentration along the ACOM radius. It can be inferred that this is due to the mutual interaction of the TA molecules.

The mutual distribution of ARN and BP10 in bulk oil can also be described by the $g^{C^*-C^*}(r)$, $g^{O^*-O^*}(r)$ and $g^{COOH-COOH}(r)$ reported in Fig. 8 for the different cases. From the comparison of Fig. 8a and Figs. 2c and 2d for the similarity of the RDFs, the two amphiphilic molecules can be considered mostly dispersed in oil for case (ii). Only slight variations in the radial distribution functions can be observed in case (iii), where the RDF reports the unfavorable direct interactions between amphiphilic molecules. In case (iv), where 8 molecules are considered, the radial distribution function reported in Fig. 8c, consistent with the density distribution functions of Fig. 7, shows a different behavior between the two TAs. $g^{C^*-C^*}(r)$ presents a peak at 0.5 nm, which confirms the previous deduction that the ARN molecules tend to associate in dimers. The subsequent mostly monotonic increase of the RDF towards unity is indicative of a uniform dispersion of the TAs in oil. On the other hand, $g^{O^*-O^*}(r)$ of case (iv) confirms that BP10 tends to locally overconcentrate as shown by the well-defined peak. From the RDF reported in Figure 8c, it can be observed that BP10 central cores do not interact directly. The BP10 carboxyl groups, instead, as shown by $g^{COOH-COOH}(r)$, directly interact with each other. It appears, therefore, that the synthetic TA tends to generate an open structure that can be described as a web, or network, where the nodes are constituted by TA cores and the TA arms, interacting via the carboxyl acids, act like bridges between the nodes. Such a network can also be visualized in Fig. 9, where 8 BP10 molecules, case (iv), are shown immersed in the oil phase. It appears that, at sufficient concentration, the molecules assemble relative to each other to generate the web. The main difference between the two amphiphilic molecules immersed in the oil phase has been reported in Fig. 2, where the conformation of a single molecule was presented. The open structure of the single molecule of BP10 is suited to generate a web since a simple distribution in the sol-

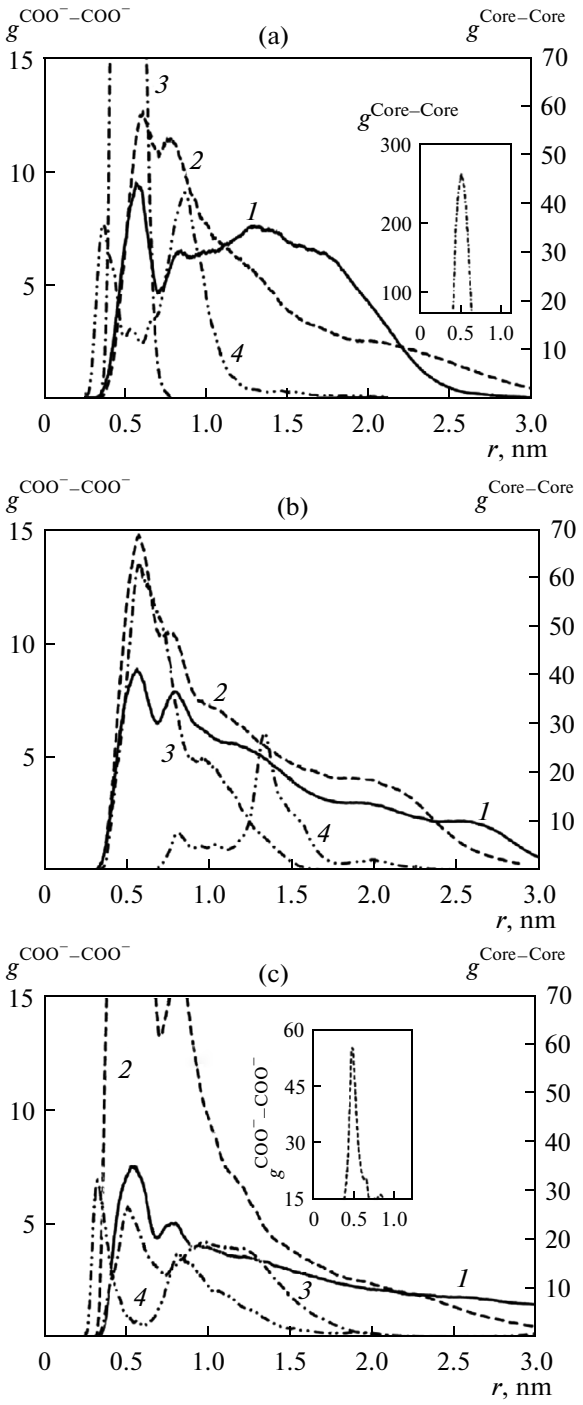

Fig. 5. RDFs for the carboxyl groups or central atoms of ARN and BP10 when (a) 2, (b) 4, or (c) 8 TA molecules are present in the bulk water phase: *1*—$g^{COO^-–COO^-}(r)$ for ARN, *2*—$g^{COO^-–COO^-}(r)$ for BP10, *3*—$g^{C^*–C^*}(r)$ for ARN, *4*—$g^{O^*–O^*}(r)$ for BP10.

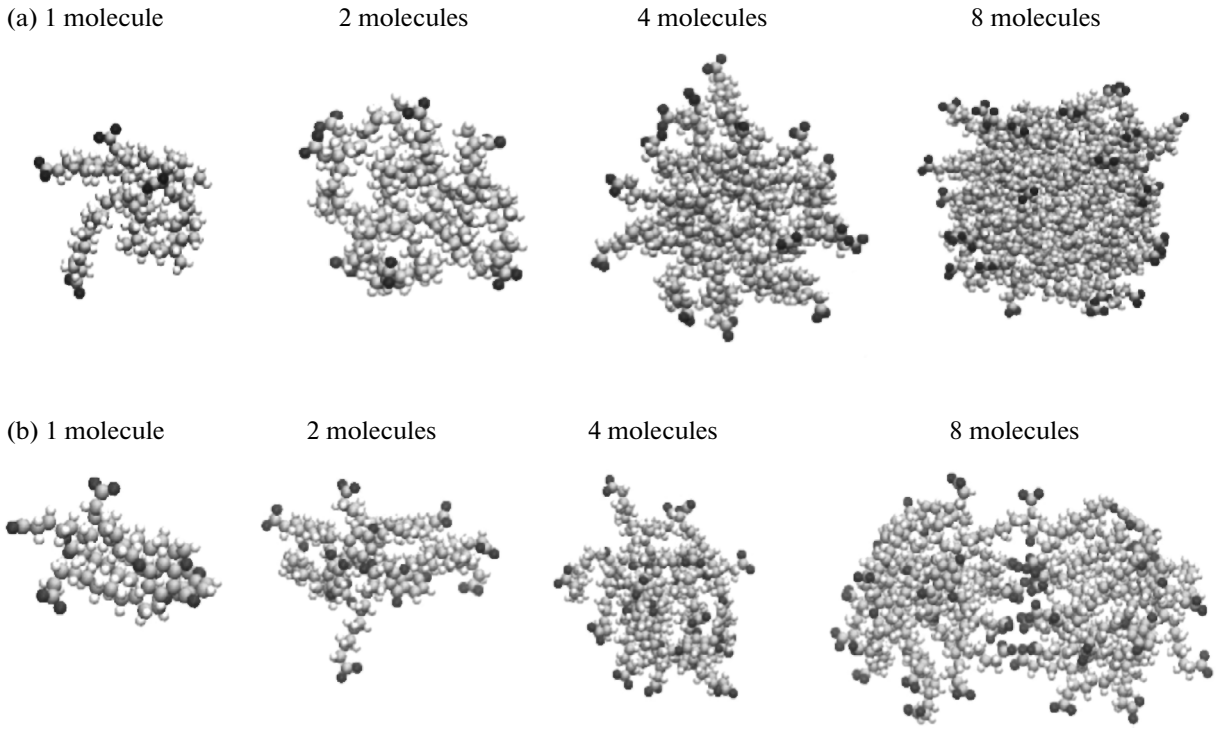

Fig. 6. Trajectory snapshots of the TA aggregation process of (a) ARN and (b) BP10 when 1, 2, 4, and 8 TA molecules are present in the bulk water phase. The darker atoms are the oxygens from the carboxyl groups, the white atoms are hydrogens, and the grey atoms are carbons.

vent is required without significant conformational changes of the molecule. It can be therefore expected that, molecules such as ARN which do not present a fully open structure, will not be able to form the observed net. It should be emphasized here that the focus of the present study is to identify the formation of aggregates. It is surely of interest, and a goal of further investigations, to study of the properties of such web-like structures and the induced modifications to the physical properties of the mixture.

4. CONCLUSION

Molecular Dynamics simulations have been employed to study the aggregation process of complex tetracarboxylic acids in bulk water and oil phases. The two molecules considered in the present study have been ARN, which is an indigenous component in crude oil and BP10, which is a model TA that is synthesizable in a laboratory. The main difference between the two amphiphilic molecules is the different rigidity of the main core that influences the accessibility of the solvent into its internal core and the interplay of the TA molecules into the formation of aggregates in the different phases. An initial analysis has been performed considering a single amphiphilic TA molecule immersed in water and oil. The conformation and solvation of the TA in the two different solvents has been studied. In water, the hydrophobic parts of both amphiphilic TA molecules tend to contract, while the carboxyl groups remain in contact with the water solvent. A hydrophobic central core of the molecule, not permeated by water and surrounded by the polar groups can be identified. The contracted inner structure does not allow water to coordinate around and solvate the central core of the TA molecule, resulting in a low solubility of the compound, which is consistent with the experimental observations [16]. In this context, single molecules of ARN and BP10 seem to behave as a sub-micellar aggregate and could be a reason why TAs form real micelles with a small aggregation number [14, 15]. In oil, each TA is fully solvated. The carboxyl atoms of the ARN tend to form more stable interactions with respect to the carboxyl groups of BP10. These solvation states result in influencing the disposition of the molecules in the oil solvent.

The simulations additionally showed that both TA molecules in the bulk water can form aggregates when more TAs are added to the system. The aggregated structures formed by the two TAs have been found to differ in their properties. It should be stressed here that the main difference between the two molecules is the rigidity of the core segment of the TA molecules. ARN aggregates present a defined inner core composed of the hydrocarbon part of the amphiphilic molecule.

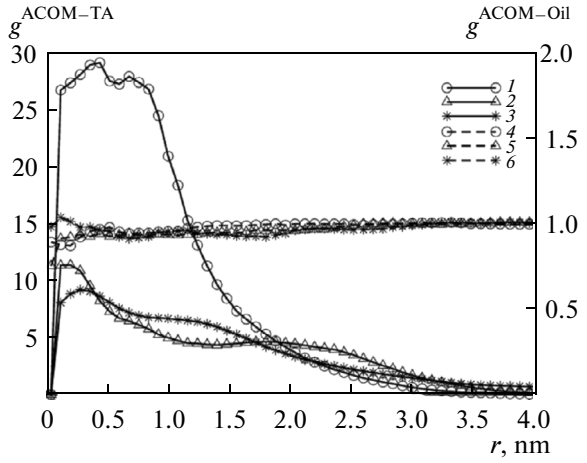

Fig. 7. RDFs for the center of mass of a BP10 aggregate with individual BP10 molecules (TA) or the solvent molecules comprising the oil phase, where *1*—$g^{ACOM-TA}(r)$ for 2 TA molecules, *2*—$g^{ACOM-TA}(r)$ for 4 TA molecules, *3*—$g^{ACOM-TA}(r)$ for 8 TA molecules, *4*—$g^{ACOM-Oil}(r)$ for 2 TA molecules, *5*—$g^{ACOM-Oil}(r)$ for 4 TA molecules, *6*—$g^{ACOM-Oil}(r)$ for 8 TA molecules.

The carboxyl groups, instead, are in contact with the water phase. In the present case of study, BP10 forms similar structures for aggregation numbers equal to 2 and 4, while for an aggregation number equal to 8, two similar structures with the properties of two micelles can be identified. Neutron scattering experiments have consistently identified BP10 micelles to be composed of 4–5 molecules at low salt concentration [12]. It appears, therefore, that under the considered conditions, BP10 cannot generate large micelles and that the growth of its aggregate depends on the cohesion of small micelles. It appears that the rigidity of the central core doesn't allow the micelle aggregate to extend towards larger aggregation numbers. The present simulations have, therefore, identified a case of study that can enable the study of micelle aggregation, stability and dispersion state in the solvent via MD by taking advantage of the small micelle dimension. The potential of this approach has been demonstrated by providing insight into the different aggregation mechanisms of two similar TAs such as ARN and BP10. MD simulations could possibly therefore describe the micelle structure, stability and aggregation as a function of pH, ionic strength, amphiphilic molecule bulk concentration, counterion type, and so on for those amphiphilic molecules.

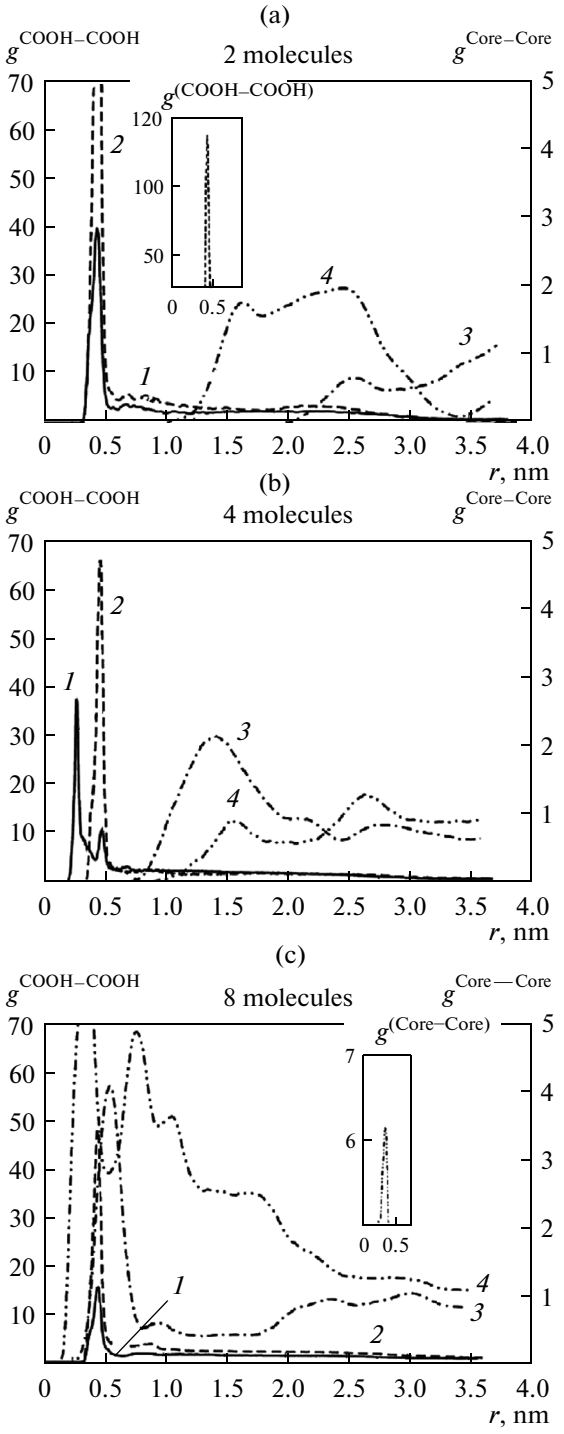

Fig. 8. RDFs for the carboxyl groups or central atoms of ARN and BP10 when (a) 2, (b) 4, or (c) 8 TA molecules are present in the bulk oil phase. In the legends: *1*—$g^{COOH-COOH}(r)$ for ARN, *2*—$g^{COOH-COOH}(r)$ for BP10, *3*—$g^{C^*-C^*}(r)$ for ARN, *4*—$g^{O^*-O^*}(r)$ for BP10.

In the second case study presented describing the behavior of ARN and BP10 in oil, their capability to form aggregated structures was investigated. The results obtained are, at an initial glance, counterintuitive. BP10 has been found to present itself mostly in an open form that is more stretched out with respect to ARN. Such a conformation is mainly kept by the TAs

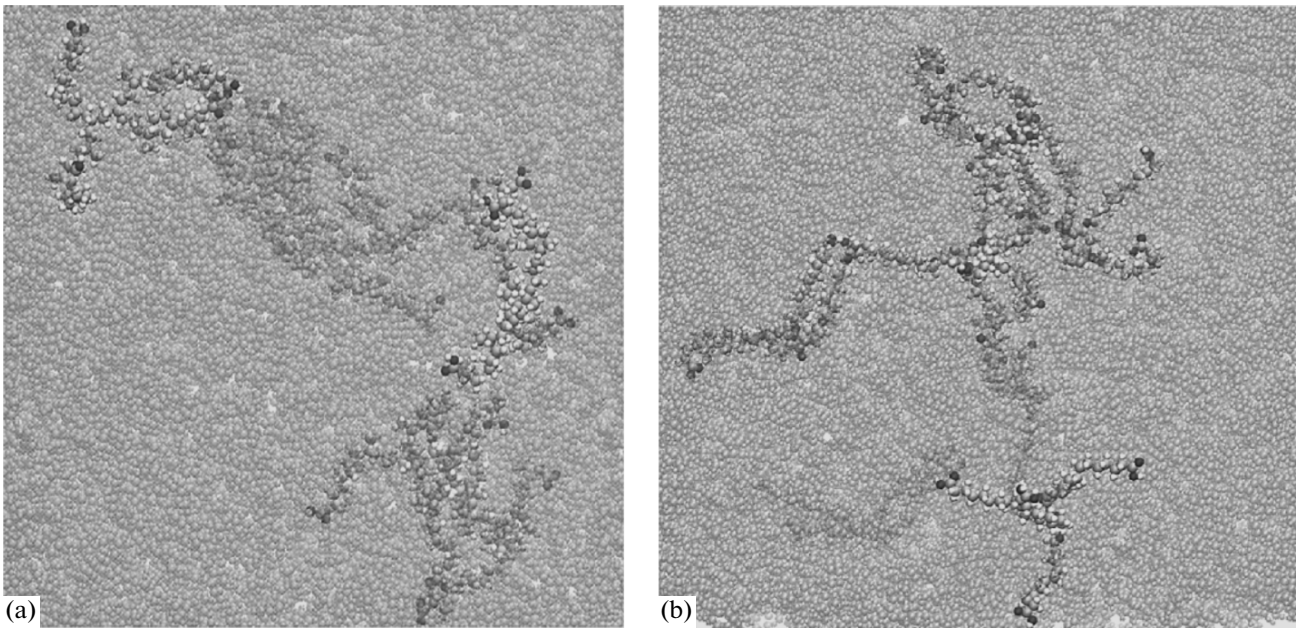

Fig. 9. Trajectory snapshots of the TA network structures of (a) ARN and (b) BP10, when 8 TA molecules are present in the bulk oil phase.

even at higher molecular concentrations, and, therefore, the amphiphilic molecule remains dispersed in the oil phase. The carboxyl groups of BP10, if present in sufficient concentration, instead, have been found to inter-molecularly interact while keeping the TA cores distant. BP10, therefore, due to its conformation in the non-polar solvent, appears to form a network, while the internal conformation of the individual molecules does not significantly change. Such an arrangement leads to a local overconcentration of the TAs which can also be defined as an 'open' aggregate, with characteristics very different from the one identified in the water phase. The structure detected in the oil phase has been here defined as web or network, where the constituent molecules are bridged to the adjacent ones via the interactions of the carboxyl groups. It appears, therefore, that the rigidity of the core structure of the TA molecules plays a determinant role in the behavior of the amphiphilic molecules and in the structure of their aggregates. The apparent ordered structure in the oil phase can strongly influence macroscopic properties of crude oils such as viscosity and conductivity. The fluid properties could be therefore altered by modifying the chemical properties e.g. arm length, polar group type, of the amphiphilic molecule considered. Further studies are intended to investigate the properties of such a network and the implications of its presence in the oil. Due to the ordered structure of the network, the physicochemical properties of the fluid, e.g. viscosity, viscoelasticity, rheological properties, conductivity can significantly differ from the sum/average of the constituent characteristics.

ACKNOWLEDGMENTS

The authors are grateful to Prof. A.I. Liapis for the helpful discussions and to the Norwegian Research Council (PETROMAKS program) and the members of the Ugelstad JIP-2 industrial consortium: Nalco Champion, Conoco Philips, ENI, Petrobras, R.E.P., Statoil, Shell, Talisman, and Total.

REFERENCES

1. McClements, D., *Food Emulsions. Principles, Practices, and Techniques.*, Boca Raton: CRC Press, 2005.
2. Baugh, T.D., Wolf, N.O., Mediaas, H., Vindstad, J.E., and Grande, K.V., *Prepr. Am. Chem. Soc., Div. Pet. Chem.*, 2004, vol. 49, p. 274.
3. Shelley, J.C. and Shelley, M.Y., *Curr. Opin. Colloid Interface Sci.* 2000, vol. 5, p. 101.
4. Ladanyi, B.M., *Curr. Opin. Colloid Interface Sci.* 2013, vol. 18, p. 15.
5. Kralova, I., Sjöblom, J., Øye, G., Simon, S., Grimes, B.A., and Paso, K., *Adv. Colloid Interface Sci.*, 2011, vol. 169, p. 106.
6. Riccardi, E., Kovalchuk, K., Mehandzhiyski, A.Y., and Grimes, B.A., *J. Disp. Sci. Technol.*, 2013, DOI 10.1080/01932691.2013.826584, in press.
7. Namani, T. and Walde, P., *Langmuir*, 2005, vol. 21, p. 6210.
8. Zhang, R. and Somasundaran, P., *Adv. Colloid Interface Sci.*, 2006, vol. 123, p. 213.
9. Stepherson, B.C., Beers, K., and Blankschtein, D., *Langmuir*, 2006, vol. 22, p. 1500.

10. Baugh, T.D., Grande, K.V., Mediaas, H., Vindstad, J.E., and Wolf, N.O., *SPE Seventh Int. Symp. on Oilfield Scale* , 2005, New York: Curran Associates, p. 8.

11. Lutnaes, F., Brandal, Ø., Sjöblom, J., and Krane, J., *Org. Biomol. Chem.*, 2006, vol. 4, p. 616.

12. Nordgård, E.L. and Sjöblom, J., *J. Disp. Sci. Technol.*, 2008, vol. 29, p. 1114.

13. Nordgaård, E.L., Magnusson, H., Hanneseth, A.-M.D., and Sjöblom, J., *Colloids Surf. A*, 2009, vol. 340, p. 99.

14. Ge, L., Simon, S., Grimes, B., Norgård, E., Xu, Z., and Sjöblom, J., *J. Disp. Sci. Technol.*, 2011, vol. 32, p. 1582.

15. Simon, S., Knudsen, K., Norgård, E., Reisen, C., and Sjöblom, *J. Colloid Interface Sci.*, 2013, vol. 394, p. 277.

16. Nordgård, E.L., *Ph.D. Thesis*, Norwegian University of Science and Technology, Trondheim, 2009.

17. Jorgensen, W.L., Maxwell, D.S., and Tirado-Rives, J., *J. Am. Chem. Soc.*, 1996, vol. 118, p. 11225.

18. Abascal, J.L.F. and Vega, C., *J. Chem. Phys.* 2005, vol. 123, p. 234505.

19. Hess, B., van der Spoel, D., and Lindahl, E., *GROMACS. User Manual. Version 4.5.4*, Uppsala: Uppsala Univ., 2010. www.gromacs.org.

20. Bussi, G., Donadio, D., and Parrinello, M., *J. Chem. Phys.*, 2007, vol. 126, p. 014101.